AALBORG UNIVERSITY

Autonomous Power Management in LVDC Microgrids based on a Superimposed Frequency Droop

Peyghami, Saeed ; Mokhtari, Hossein; Blaabjerg, Frede

Link to publication from Aalborg University

Autonomous Power Management in LVDC Microgrids based on a Superimposed Frequency Droop

Saeed Peyghami[1], *Student Member, IEEE,* Hossein Mokhtari[1], *Senior Member, IEEE,* and Frede Blaabjerg[2], *Fellow, IEEE*

Abstract— In this paper a novel droop approach for autonomous power management in low voltage dc microgrids based on a master-slave concept is presented. Conventional voltage-based droop approaches suffer from poor power sharing due to line resistance effects on a virtual resistance, which is solved a by introducing a communication system to increase the current sharing accuracy. In this paper, a virtual frequency is superimposed by the master units, and slave units determine their output power according to the corresponding frequency-based droop characteristics. Unlike the voltage-droop methods, the proposed virtual frequency-droop approach can be applied for proportional power management among the energy units and loads in the microgrid without utilizing any extra communication system. The effectiveness of the proposed scheme is evaluated by simulations and further validated by experiments.

Index Terms— DC Microgrid, Autonomous Control, Power Management, Interlinking Converter.

I. INTRODUCTION

The concept of ac/dc Microgrids (MGs) has been proposed in recent years to enhance the reliability, power quality and efficiency of the distribution power systems [1]–[6]. Future distribution systems will consist of many interconnected ac and dc MGs, which are dynamically decoupled from the each other [7], [8]. Integrating Renewable Energy Resources (RERs) and storages into the distribution systems to enhance the overall reliability and efficiency, requires proper power sharing algorithms by employing the MG and also smart grid technologies [1], [5], [9]–[11]. Furthermore, dc MGs are more applicable, reliable and efficient systems to integrate many power sources and loads, such as PhotoVoltaic (PV) modules, Fuel Cell (FC) units, batteries, motor driven loads, and full converter based generators (i.e. micro-turbines and wind turbines), which naturally have a dc coupling. Dc MGs are connected to the grid through a power electronic converter also called Interlinking Converter (IC), and hence they are naturally decoupled from the utility grid. Therefore, an independent power sharing control from the utility side can be employed in order to control the load sharing among different energy units in the MG as well as the power flow between the MG and the utility through the IC (/ICs).

So far, autonomous power management strategies based on voltage-droop methods have been presented to control the load sharing among different energy units in dc MGs [12]–[19]. In [12], a voltage-based droop approach is considered for dispatchable units as master units and the other units including battery storages and non-dispatchable resources are operating as a slave converters. However, the dc bus is common for all units and the dc voltage has the same value for all converters because of neglecting the line impedances. Furthermore, a voltage-droop based control approach is presented with equal line resistances in [13], [14], and without considering line resistance effects in [15]–[17]. Moreover, the voltage droop-based control system in [13], [14] relies on only one master unit in each operating modes, which affects the system resiliency. An autonomous power sharing approach is also presented in [18] based on the droop approach reinforced by a secondary layer employing communication among the converters. Voltage-based droop approaches rely on the dc link voltage, where the dc link voltage is a local variable and it does not have the same value through the MG in order to coordinate the different converters. Therefore, in the case of taking into account the line resistances, the performance of the voltage-based droop methods is not satisfactory [20]–[25]. In order to increase the accuracy of the load sharing, large droop gains should be employed, where the larger droop gains cause higher voltage drop and may lead to dynamic instability. To solve these issues, average current sharing approaches reinforced by communication infrastructures have been presented in [26]–[29], which may affect the overall system reliability and stability [24].

In order to overcome the aforementioned issues, a novel autonomous power sharing control strategy based on a merged master-slave and frequency droop concepts is proposed in this paper. Distributed storages are considered as master units to inject a small ac voltage with a frequency (f_v) proportional to the corresponding output currents. Other units locally extract the frequency to control the output currents according to the proposed droop characteristics. Since the frequency has the same value through the MG, it can be employed not only to coordinate all types of energy units but also to curtail the non-critical loads. The proposed control strategy and operating modes are explained in Section II. In Section III, the proposed converter control structures are discussed, and the small signal stability analysis are given in Section IV. The simulations and experiments validate the control system viability in Section V

---

[1] Saeed Peyghami and Hossein Mokhtari are with the Department of Electrical Engineering, Sharif University of Technology, Iran (e-mail: saeed_peyghami@ee.sharif.edu, mokhtari@sharif.edu).

[2] Frede Blaabjerg is with the Department of Energy Technology, Aalborg University, Denmark (e-mail: fbl@et.aau.dk).
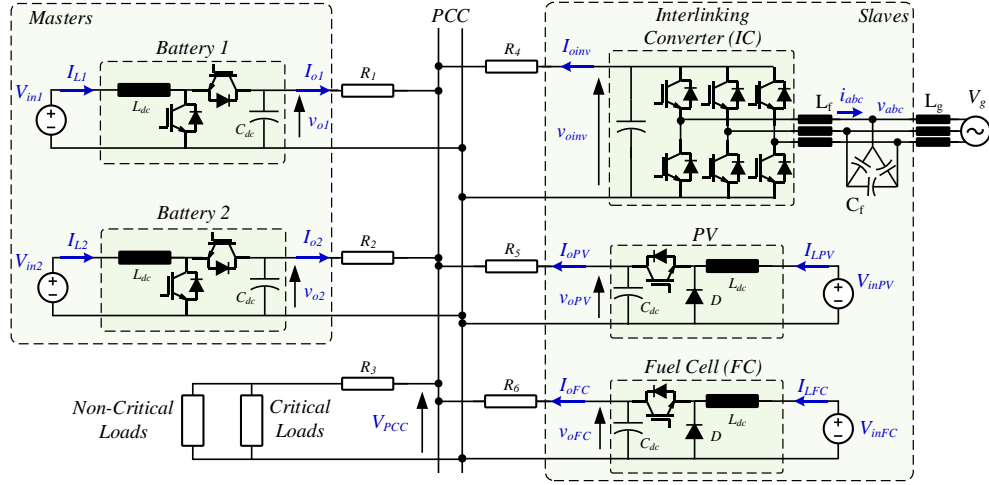
Fig. 1. A typical dc MG including battery storages, grid interlinking converted, non-dispatchable DGs (PV), dispatchable DGs (FC), and localized critical and non-critical loads.

and Section VI respectively. Finally, the achievements are summarized in Section VII.

II. PROPOSED FREQUENCY-BASED DROOP CONTROL APPROACH

The proposed control system relies on the merged master-slave approach and frequency-droop method. The battery storages are considered as a master unit introducing a frequency superimposed onto the dc link voltage. According to [30], the master units are coordinated together based on the frequency droop approach like the grid supporting voltage source converters in ac grids [31]. The other units including dispatchable and non-dispatchable units operate as a grid supporting current source converter by utilizing the superimposed frequency of the dc link voltage and proposed droop characteristics. The main structural idea of the control strategy and operating modes are explained in the following.

A. Control Approach and Operating Modes

A typical dc MG with storages, dispatchable (FC and IC) and non-dispatchable (PV) units are shown in Fig. 1. Two battery storages are considered as the masters and other units are the slaves. The proposed droop characteristics for the masters and slaves are shown in Fig. 2. The master units modulate a small ac voltage superimposed to the dc voltage with a frequency (f_v) determined by (1) which is graphically shown in Fig. 2(a).

$$f_v = f_0 - \frac{f_{max} - f_{min}}{I_d^{max} + I_{ch}^{max}} I_B = f_0 - K_b I_B, \quad (1)$$

Where f_{max} and f_{min} are the maximum and minimum frequencies, I_{ch}^{max} and I_d^{max} are the maximum charging and discharging currents of the battery, and I_B is the output current of battery converter. f_{max} and f_{min} should be selected such that the overall system stability can be guaranteed. Furthermore, the master units can be coordinated together with a droop concept presented in [30] and will be explained in the next section.
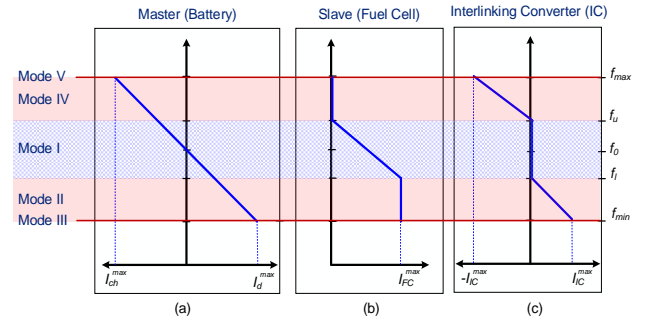

Fig. 2. Proposed droop control scheme: (a) droop characteristic of battery, (b) droop characteristics of Fuel Cell, and (c) droop characteristic of Interlinking Converter.

As shown in Fig. 2(a), the storage units are working in all operating modes. If the $f_v > f_0$ it is in the charging mode and once $f_v < f_0$, it is ready to discharge. Moreover, the energy level of the battery needs to be controlled to ensure proper supporting of the MG. Hence, the proposed droop equation of the battery should be tuned based on the State of Charge (SoC) level of the battery. This procedure is explained in the subsection B.

According to the superimposed frequency by the masters, which is related to the demand of the MG, five operating modes can be considered as shown in Fig. 2.

Mode I: As shown in Fig. 2(b), the frequency f_v is between f_u and f_l, and the loads are demanded by the local energy units including FC, PV and battery, and the exchanged power with the utility grid is zero (i.e., $I_{IC} = 0$). As shown in Fig. 2(b), the output current of the FC can be found as

$$I_{FC} = \frac{I_{FC}^{max}}{f_l - f_u}(f_v - f_u) = K_{FC}(f_v - f_u), \quad (2)$$

and the PV is working in the MPPT mode. f_u and f_l should be selected such that the overall system stability can be guaranteed.

Mode II: in this mode, the loads are exceeded to the rated current of the FC and the current of the PV, thus, the

frequency drops down $f_v < f_l$, and the MG needs to be supported by the grid through the IC. According to the droop characteristics shown in Fig. 2(c), the current of the IC can be calculated as:

$$I_{IC} = \frac{I_{IC}^{max}}{f_{min} - f_l}(f_v - f_l) = K_{IC}(f_v - f_l), \qquad (3)$$

Mode III: if the load exceeds the rated current of all units, the load shedding should be applied to non-critical loads. They can be disconnected from the grid once the frequency $f_v < f_{min}$.

Mode IV: whenever the output current of the PV exceeds the local load, it can be injected to the grid and the battery. Hence, in this condition the virtual frequency f_v is between f_u and f_{max}, the FC is in the off state and the excess current is injected into the grid and the battery. In this mode, the IC current can be found as:

$$I_{IC} = -\frac{I_{IC}^{max}}{f_{max} - f_u}(f_v - f_u) = K_{IC}(f_v - f_u), \qquad (4)$$

Mode V: if the output current of the PV exceeds the maximum currents of the IC, battery and load, the corresponding control system needs to be switched to the non-MPPT mode to fix the frequency at $f_v = f_{max}$. The superimposed frequency by the masters as grid supporting voltage source converters are employed by the slaves as grid supporting current source units. Like the frequency droop approach in ac grids [31], applying the same approach for the dc MG can properly carry out the load sharing among the different energy units. Since the frequency has the same value through the MG, the proposed approach will not be affected by the line resistances. Hence, the conventional droop approach problems including inaccurate load sharing and voltage drop introduced by the line and virtual droop resistances can be solved by employing the proposed frequency droop approach.

B. Battery Droop Tuning

In order to increase the availability of the battery energy as a master unit to support the MG, a charging and discharging procedure has to be controlled. Most batteries have a form of EMS to monitor local quantities like voltages, currents, temperature, humidity, and etc., before concluding on the present SoC, life cycle and other operating details of the batteries. However, a simple method for calculating the SoC level of a battery is a coulomb counting approach [17], [28], which gives the SoC level of the battery at (t) by integrating the battery current as:

$$SoC(t) = SoC(0) - \frac{\eta}{C}\int_0^t I(\tau)\,d\tau, \qquad (5)$$

where SoC(0) is the initial SoC of the battery, η is the charging and discharging efficiency and C is the total battery capacity. The calculated SoC can be used to tune the charging and discharging characteristics of the batteries defined in (1), which can simply be performed by adjusting I_d^{max} and I_{ch}^{max} [32]. In this paper three states are considered for tuning the droop characteristics as shown in Fig. 3(a) including Fully Charged Condition (FCC) for 80 % < SoC < 100 %, Half Charged Condition (HCC) for 10 % < SoC < 90 % and Fully
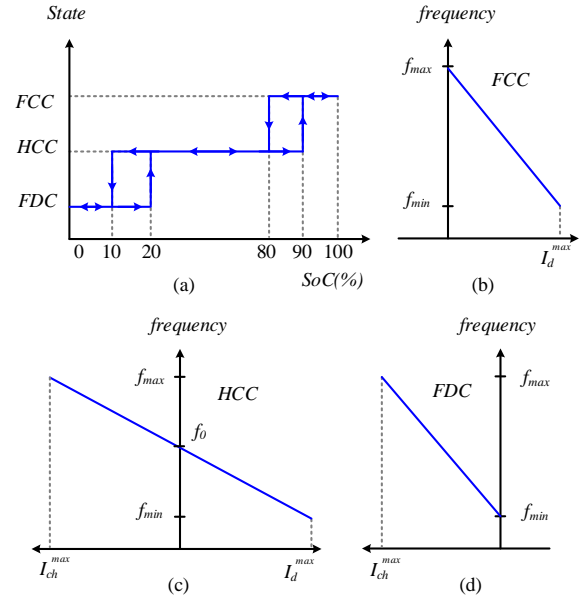

Fig. 3. Battery droop tuning procedure by corresponding energy management system, (a) state selection strategy based on SoC level of battery – Fully Charged (FCC), Half Charged (HCC), Fully Discharged (FDC) ,(b) droop characteristics for FCC condition (80 % < SoC < 100%), (c) HCC condition (10 % < SoC < 80%), and (d) FDC Condition (0 % < SoC < 20%).

Discharged Condition (FDC) for 0 < SoC < 20 %. According to the SoC state of the battery, the corresponding droop characteristics are adjusted by the control system as shown in Fig. 3(b) for the FCC, Fig. 3(c) for the HCC, and Fig. 3(d) for the FDC. In practice, the capacity of the batteries are high enough to support the critical loads of MG for an acceptable period. Therefore, the parameter C in (5) is large and the variation of SoC is very slow [28]. Hence the switching among the different states are dynamically slow in practice, and it will not affect the overall stability of the system [28].

III. CONTROL STRUCTURE OF CONVERTERS

As already mentioned, the batteries are operating as a master for regulating the dc link voltage and introducing a frequency where the other units are working as a slave. The proposed control structure for the MG converters is shown in Fig. 4 and explained in the following.

A. Control of Master Units

Master units are responsible for generating a frequency as a global control variable for all energy units as well as forming the dc link voltage. In this paper, the battery storages are considered as the master units, which are connected to the grid through a bidirectional dc/dc converter as shown in Fig. 1. Furthermore, the number of Master units has to be at least equal to two based on the N-1- criterion, where losing one master doesn't affect the system operation. The control structure of the master units are shown in Fig. 4(a), where the kth converter modulates an ac voltage ($\tilde{v}$) superimposed onto the dc voltage [30]. The frequency of the ac voltage is proportional to the corresponding dc current. According to [30], the ac voltages introduce an ac power flow in the grid, which is proportional to the output current of the converters.

Therefore, it can be employed to adjust the dc voltage of master units. As seen in Fig. 4(a), the phase angle (δ_k) of the ac voltage at the output terminal of the kth converter is

$$\delta_k(t) = \int_0^t 2\pi(f^* - K_{bk}i_{ok}(\tau))\,d\tau \,, \tag{6}$$

where f^* is the set point frequency, d_{fk} is the droop gain, i_{ok} is the output current of kth converter. The rated frequency f^* needs to be smaller than the bandwidth frequency of the voltage control loop of master converters to be properly generated [30]. Considering two master units connected to the grid, the relative phase between the corresponding ac voltages can be found as:

$$\delta(t) = \delta_1(t) - \delta_2(t) = \int_0^t 2\pi(K_{b2}i_{o2}(\tau) - K_{b1}i_{o1}(\tau))\,d\tau \,. \tag{7}$$

Therefore, if the output currents are not proportional to the droop gains, a phase angle will be appear in the output ac voltages. From the ac power flow theory, the phase angle makes an ac power flow in the grid. Considering the load impedances higher than the line impedances, the ac power only flowed between the converters [30]. This ac power can be employed to adjust the dc voltages to have a proportional current sharing between the two masters [30]. Hence, utilizing the merged ac/dc droop characteristics causes appropriate load sharing between the master units. Reference [30] describes the control strategy of the master units in details.

In the MG, the master units are operating like a grid supporting voltage source converters in the ac grids [31] in order to form the voltage and frequency of the MG. The other slave units like grid supporting current source converters in ac grids [31] utilize the superimposed frequency by the master units in order to find the output current reference based on the proposed frequency-droop characteristics shown in Fig. 2. The control structure of the slave units are explained in the following.

B. Control of Dispatchable Units

The output power of dispatchable units like FC and IC can be controlled to generate a desired power. In droop mode operation, the corresponding output power reference is determined by the MG demand and the droop characteristics. The control structure of the IC and FC are shown in Fig. 4(b) and (c) respectively. The superimposed frequency is estimated by a Frequency Locked loop (FLL) from the output voltage, and hence, the current reference for the inner loop is determined based on the droop characteristics shown in Fig. 2(b) and (c) respectively for FC and IC. The dc and ac power of the IC (P_{dc}, P_{ac}) can be defined as (8), where the v_{oinv} and i_{oinv} are the dc voltage and current of the IC and V_d and i_d are the d-axis component of the ac side voltage and current of the IC. In this paper, i_d is proportional to the active power and i_q is proportional to the reactive power as shown in Fig. 4. Furthermore, ac side reactive power control is not discussed in this paper, and hence the reference current of q- axis i_q^* is set to zero.

$$\begin{aligned} P_{dc} &= v_{oinv}I_{oinv} \\ P_{ac} &= 1.5V_d i_d \end{aligned} \tag{8}$$

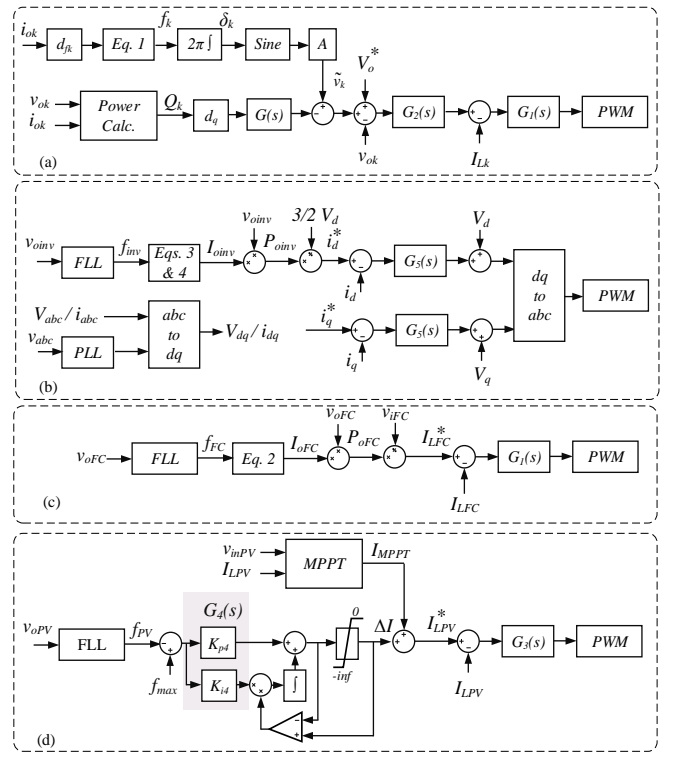Therefore, by neglecting the converter losses, the d-axes current reference of the IC can be determined as (9).

Fig. 4. Control structure of the (a) k^{th} battery, (b) Interlinking Converter (IC), (c) Fuel Cell (FC), and (d) PV array – $Gj(s) = k_{pj}+k_{ij}/s$ is a proportional-integrator regulator, FLL: Frequency Locked Loop, PLL: Phase Locked Loop, MPPT: Maximum Power Point Tracking.

$$i_d^* = \frac{v_{oinv}I_{oinv}}{1.5V_d} \tag{9}$$

Similar to the IC, the input and output power (P_{iFC}, P_{oFC}) of the FC converter shown in Fig. 1, can be determined as (10), where the input and output voltage of FC are denoted as v_{iFC}, v_{oFC}, and the input and output current of FC are defined as I_{iFC} and I_{oFC}. Furthermore, the input current of the FC in the boost converter is equal to the dc inductor current (I_{LFC}).

$$\begin{aligned} P_{iFC} &= v_{iFC}I_{iFC} \\ P_{oFC} &= v_{oFC}I_{oFC} \end{aligned} \tag{10}$$

Therefore, the dc current reference of the inner control loop of FC can be determined as:

$$I_{LFC}^* = I_{oFC}\frac{v_{oFC}}{v_{iFC}} \,. \tag{11}$$

C. Control of Non-Dispatchable Units

Non-dispatchable units like PV are operating in MPPT mode during the normal operation condition, i.e., Mode I to Mode IV. Hence, the corresponding converter injects the MPPT current (power) into the grid. Once the frequency goes over the maximum limit (f_{max}), the converter needs to bring down the output power to decrease the frequency. The proposed control structure of the PV array as a MPPT-based unit is shown in Fig. 4(d). Until the frequency is smaller than f_{max}, as shown in Fig. 4(d), the output of the PI controller is saturated at zero and the integrator is deactivated. Hence ΔI (the output of the PI controller) is equal to zero and the converter operates in MPPT mode. Once the frequency goes larger than f_{max}, the

PI controller is activated and the reference current is decreased to fix the frequency at f_{max}. Therefore, without using a supervisory controller to make a decision between two MPPT and non-MPPT approaches presented in [17], [28], the PV converter can be seamlessly switched from MPPT to non-MPPT mode, which is here called frequency control mode.

IV. SMALL SIGNAL STABILITY

In this section, the dynamic behavior of the control system is investigated by employing the small signal stability analysis. As shown in Fig. 2, in each mode of operation, only one slave unit is working in droop mode. Hence, in order to analyze the dynamic behavior of the system in each mode, the droop characteristics of the corresponding slave unit with the droop characteristics of the master units needs to be considered. The small signal model of the droop controlled slave unit can be represented as:

$$\Delta I_{slave} = -G_{slave}(s)G_{FLL}(s)\frac{\Delta\omega}{2\pi}, \qquad (12)$$

where, $\Delta\omega = 2\pi\Delta f$, and

$$G_{slave} = \begin{cases} -K_{FC}\dfrac{G_i(s)G_{id}(s)}{1+G_i(s)G_{id}(s)} & Mode\,I \\[2mm] -K_{IC}\dfrac{1}{1+sT_i} & Mode\,II, IV \\[2mm] -G_f(s)\dfrac{G_i(s)G_{id}(s)}{1+G_i(s)G_{id}(s)} & Mode\,V \end{cases}, \quad (13)$$

where $G_f(s) = k_{p4} + k_{i4}/s$ is the frequency controller of the PV shown in Fig. 4(d). $G_{FLL}(s)$ is the transfer function of the FLL, which can be modeled as a first order delay as:

$$G_{FLL}(s) = \frac{1}{1+sT_{FLL}}. \qquad (14)$$

According to [30], and considering the control system shown in Fig. 4, the characteristic equation of the closed loop system can be found as:

$$\xi s + 2\pi K_{b1}(\lambda\beta - 1) = 0, \qquad (15)$$

where

$$\xi = \frac{\gamma + R_0(1+\beta)}{R_0 G_{slave}(s)s}, \qquad (16)$$

$$\beta = \frac{2\alpha + r_1}{2\lambda\alpha + r_2}, \qquad (17)$$

$$\gamma = \alpha - \beta(\lambda\alpha + r_2), \qquad (18)$$

$$\lambda = \frac{K_{b2}}{K_{b1}}, \qquad (19)$$

$$\alpha = 2\pi K_{b1}d_q K_\delta G(s)/s, \qquad (20)$$

where as shown in Fig. 4(a) and discussed in [30], $G(s)$ is a low pass filter by a cut-off frequency of 10 Hz for rejecting the oscillations of the measured power, and d_q and K_δ are defined in [30]. R_0 is the load resistance in steady state in which for constant power load (with voltage of V_0 and power of P) can be defined as:

$$R_0 = \frac{V_0^2}{P}. \qquad (21)$$

TABLE I: Parameters of the simulated MG and the control system

Definition	Symbol	Value	Definition	Symbol	Value
Rated current of Batteries	I_d^{max} – I_{ch}^{max} (A)	5	Maximum frequency	f_{max} (Hz)	51
Rated current of FC	I_{FC}^{max} (A)	5	Upper frequency	f_u (Hz)	50.25
Rated current of IC	I_{IC}^{max} (A)	10	Lower frequency	f_l (Hz)	49.75
Rated power of PV	P_{MPPT} (kW)	3	Minimum frequency	f_{min} (Hz)	49
Nominal dc Voltage	V_{dc} (V)	400	Voltage-power gain	d_q	20
Rated frequency	f_o (Hz)	50	Feeder 1, 3	$R_{1,3}(\Omega)$	0.2
AC grid Voltage	$Vabc$ (V_{peak})	180	Feeder 2, 5	$R_{2,5}(\Omega)$	0.15
Small AC Voltage	$Peak$-$Peak$ (V)	2	Feeder 4, 6	$R_{4,6}(\Omega)$	0.2
Battery Current regulator Voltage regulator	$(k_{p1}+k_{i1}/s)$ $(k_{p2}+k_{i2}/s)$	0.2 + 5/s 0.05 + 1/s	PV Current regulator Voltage regulator	$(k_{p3}+k_{i3}/s)$ $(k_{p4}+k_{i4}/s)$	0.05 + 1/s 0.35+2/s
FC Current regulator	$(k_{p1}+k_{i1}/s)$	0.05 + 1/s	Inverter Current regulator	$(k_{p5}+k_{i5}/s)$	0.01 + 0.04/s
Boost converter components	L_{dc} (mH), C_{dc} (µF)	2, 560	Inverter components	C_{dc} (µF), L_f (mH) C_f (µF)	220, 2, 560

For the microgrid shown in Fig. 1 with the control parameters given in Table I, the closed loop poles of the system can be found by employing the characteristic equation (15). The dominant eigenvalues trace of the closed loop system is shown in Fig. 6 for different operating modes. In the case of fully charged/discharged batteries, as shown in Fig. 3, the droop gain is two times the half charged condition. Hence the pole places of the system for FCC/FDC is shown in Fig. 6(a) and for HCC is shown in Fig. 6(b). Furthermore, the system dynamic behavior is the same for Mode II and IV since the droop gain of IC has the same value in these modes. Moreover, when the system enters into Mode III, the load shedding strategy needs to be applied to the non-critical loads. Therefore, after load shedding, the system will be operated in one of the droop controlled modes taking into consideration the shed loads, where the system dynamic response can be determined in the new mode described by (12) and (13).

V. SIMULATION RESULTS

In order to evaluate the proposed control strategy, the dc MG shown in Fig. 1 is considered with the parameters given in Table I. Simulation results are presented in the following in order to validate the performance of the control system at different loading and sourcing conditions.
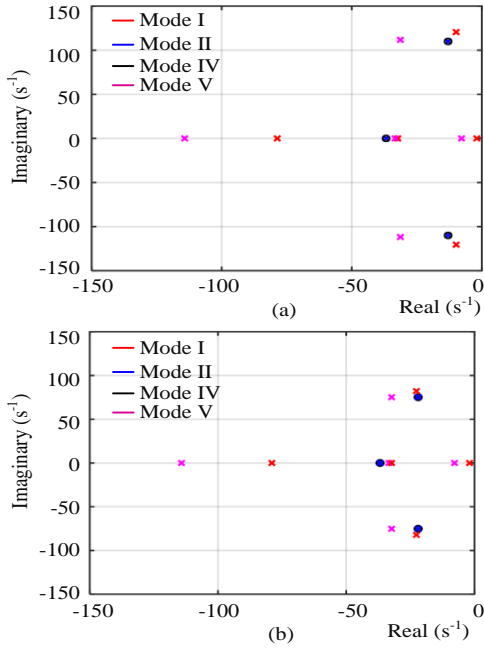
Fig. 5. Closed loop pole placement of the microgrid in (a) Fully Charged/Discharged Condition (FCC/FDC), (b) Half Charged Condition (HCC).

In the first simulation, a 4 *kW* load is connected to the system. The batteries are half charged and the droop characteristics are adjusted like the one shown in Fig. 3(c). The PV is operating at MPPT mode. As shown in Fig. 6(a), the frequency is equal to 50 *Hz*, hence the system is operating in Mode I. According to Fig. 2, in *f* = 50 *Hz*, the inverter and batteries need to be off and the load has to be supported by the PV and FC. As it can be seen from Fig. 6(b), the load is supplied by the PV and FC. Moreover, the output current of the inverter and batteries are equal to zero.

Another 4 *kW* load is turned on at *t*= 1*s*, and the frequency is settled at 49.5 *Hz* as shown in Fig. 6(a). Therefore, the system operates in Mode II, and as it can be seen from Fig. 6(b), the FC generates the rated current. The FC, inverter and batteries supply the load of microgrid. By connecting another 4 *kW* load at *t* = 3 *s*, the system still operates in Mode II. The incremental load is proportionally supported by the batteries and the inverter based on the corresponding droop characteristics defined in Fig. 2, and the FC is fully loaded. By decreasing the output power of the PV at *t* = 5 *s*, the system goes to Mode III and the frequency is equal to 49 *Hz* as shown in Fig. 6(a). The batteries, inverter and the FC operate at rated current, and hence the system is heavily loaded. The output power of the PV is further decreased at *t* = 7 *s*, and the generation capacity is lower than the system load. Therefore, the frequency goes below f_{min} = 49 *Hz*, and a non-critical load is disconnected in order to restore the frequency to a normal value. As it can be seen from Fig. 6(a), the system is operating in Mode II after load shedding, and the power sources are supporting the load based on the corresponding droop characteristics. The load bus voltage is shown in Fig. 6(c) implying an acceptable voltage regulation in the load bus. Moreover, the superimposed ac ripple onto the dc voltage can be seen in the load bus containing the power sharing information i.e., ac ripple frequency.
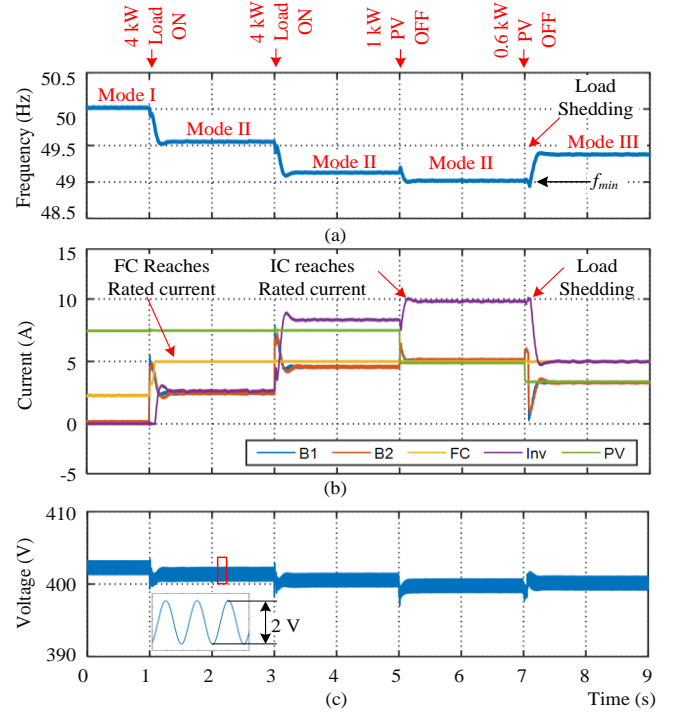

Fig. 6. Superimposed frequency, output current of power sources and load bus voltage. The system is operating in Modes I, II and III, the batteries are half charged and the PV is working at MPPT – The load shedding is done at *t* = 7 *s*.
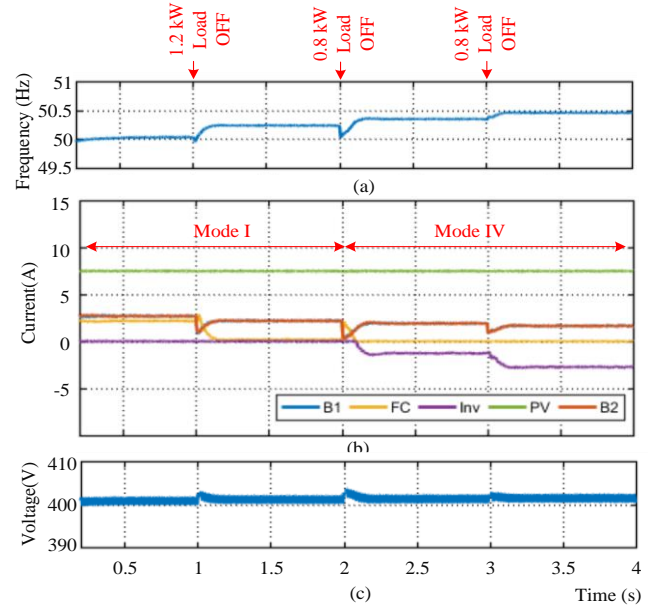

Fig. 7. Superimposed frequency, output current of power sources and load bus voltage. The system is operating in Modes I, IV, the batteries are fully charged and the PV is working at MPPT.

In the next simulation study, the batteries are considered to be fully charged and the corresponding droop characteristics are considered as the one shown in Fig. 3(b). Furthermore, the PV is operating in MPPT mode. A 6 *kW* load is connected and supplied by the PV, FC and batteries as shown in Fig. 7. The system frequency is equal to 50 *Hz* and the system is operating in Mode I. Therefore, according to the droop characteristics shown in Fig. 2(c), the output power of the inverter should be zero. Moreover, the output current of FC and batteries are

determined by the corresponding droop characteristics in Fig. 2(b) and Fig. 3(b) respectively. The load sharing results are shown in Fig. 7(b) implying that the load is supported by the PV, FC and batteries.

The load is decreased by 1.2 *kW* at *t* = 1 *s*, and the frequency is settled at 50.25 *Hz*. Therefore the FC is turned off and load is supported by the batteries according to Fig. 2(b) and Fig. 3(b). Further decrease in load at *t* = 2 *s* increases the frequency to 50.4 *Hz* and the system operates in Mode IV. Therefore, according to Fig. 2(c) the inverter needs to inject the excess power of the MG into the grid. By decreasing the load at *t* = 3 *s*, the injected power into the grid by the inverter is increased. The load bus voltage is shown in Fig. 7(c) implying an acceptable voltage regulation in the load bus.

In order to further evaluate the control system, FC is considered to be turned off, and power injection into the grid is not allowed by the TSO. Moreover, one of the batteries are fully charged and another one is half charged. Therefore, the system is only supported by the batteries and PV. At first the system is operating in Mode I with 5.3 *kW* load. The system frequency and output current of the power sources are shown in Fig. 8(a) and (b). As it can be seen in in Fig. 8(a), the frequency is under 50 Hz, hence the batteries are supporting the load. Since one of the batteries is half charged, the corresponding current (see Fig. 8(b)) is half of the other one following the droop characteristics shown in Fig. 3. At *t* = 0.8 *s*, the first battery is turned off, and the system goes to Mode III. A 2.6 *kW* load is disconnected at *t* = 1.6 *s*. The frequency is increased to be above 51 *Hz*. Therefore, the generation capacity is more than the system load and the PV must operate at lower power than the MPPT power. As it can be seen in Fig. 8(b), after 0.2 *s*, the frequency control loop shown in Fig. 4(d) is activated. Therefore, the output current of the PV is decreased in order to keep the frequency at f_{max} = 51 *Hz*, and the system goes into Mode V, and the load is supported by the PV. Furthermore, the load bus voltage is shown in Fig. 8(c) implying an appropriate voltage regulation in Mode V.
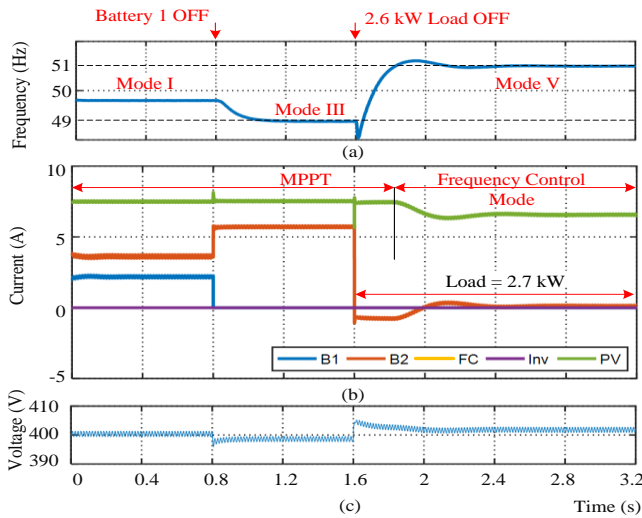

Fig. 8. Superimposed frequency, output current of power sources, and load bus voltage. The system is operating in Modes I, III, and V. The batteries are fully charged, the FC is turned off and the inverter is not allowed to inject power into the grid. The PV is working in MPPT mode and at *t* = 1.6 s, the PV switches to the frequency control mode.

The performance of the control system in different Modes defined in Fig. 2 is evaluated with different simulations, and power sharing among different energy units are illustrated at different loading and sourcing conditions.

VI. EXPERIMENTAL RESULTS

In order to validate the effectiveness of the proposed approach, experimental tests with a scaled-down laboratory prototype is performed, and the control system performance is evaluated in some operation points. The photograph of the test system is shown in Fig. 9 including two synchronous boost converters and one three phase inverter. One of the dc converters is considered as a battery and another one is considered as a PV and/or FC during the tests. The inverter is also grid interface. The system and control parameters are given in TABLE II, and the test results are reported in the following.
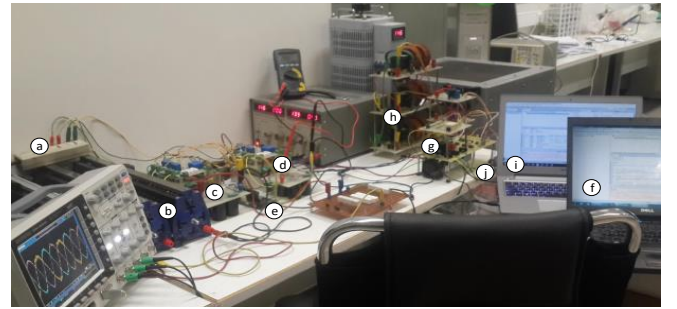

Fig. 9. Photograph of the implemented hardware setup (a) input dc power for dc/dc converters, (b) dc load, (c, d) dc/dc boost converters, (e) DSP for boost converters, (f) control center of boost converters, (g) three phase inverter, (h) filter of inverter, (i) control center of inverter, and (j) DSP for inverter.

TABLE II: Parameters of the implemented MG and control system

Definition	Symbol	Value
	Rated current (A)	2.5
	Inner voltage regulator $(k_{p1} + k_{i1}/s)$	0.2 + 5/s
Boost Converter for battery	*Inner current regulator* $(k_{p2} + k_{i2}/s)$	0.05 + 1/s
	Droop at FCC/FDC	0.8
	Droop at HCC	0.4
	L_{dc} *(mH)*, C_{dc} *(µF)*	2, 560
	Rated MPPT Current (A)	2.5
Boost Converter for PV	*Inner current regulator* $(k_{p3} + k_{i3}/s)$	0.05 + 1/s
	Frequency regulator $(k_{p4} + k_{i4}/s)$	0.35+2/s
	L_{dc} *(mH)*, C_{dc} *(µF)*	2, 560
	Rated Current (A)	2.5
Boost Converter for FC	*Inner current regulator* $(k_{p1} + k_{i1}/s)$	0.05 + 1/s
	Droop gain	5
	L_{dc} *(mH)*, C_{dc} *(µF)*	2, 560
	Rated current (A)	2.5
Inverter	*Inner current regulator* $(k_{p5} + k_{i5}/s)$	0.01 + 0.04/s
	Droop gain	2.5
	C_{dc} *(µF)*	220
	L_f *(µH)*, C_f *(µF)*	1.2, 22
Feeder resistances	*R (Ω)*	1
Injected frequency	f_o *(Hz)*	50
Nominal dc Voltage	V_{dc} *(V)*	100
AC grid Voltage	$Vabc$ (V_{peak})	60
Small AC Voltage	*Peak-Peak (V)*	1

A. Operation of FC and battery and effect of SoC level:

In this case, the battery and FC are connected to a 100 *W* load, and the battery is fully charged. As shown in Fig. 10(a), only the battery supplies the load, and the FC's current is equal to zero. The system is operating in Mode IV. Once the load is changed to 200 *W*, the FC starts to supply the load as well as shown in Fig. 10(a). In this case, the battery is considered to be fully charged and the corresponding droop characteristics is like the one shown in Fig. 3(b) with a slope of 0.8. Since the droop gain of the battery is 0.8 and the FC is 2.5, the battery supplies more power. In this condition, the system is operating in Mode I. However, once the SoC level of battery is decreased, the corresponding droop characteristics is changed to Fig. 3(c). Now, both battery and FC have the same droop gains and needs to support the equal power/current as shown in Fig. 10(b) implying an appropriate dynamic response due to the SoC level variation.

B. Operation of battery and PV and effect of SoC level:

In this test, the PV is working in MPPT mode, and the battery is half charged. The load is 145 W and the system is working in Mode IV. Once the battery becomes fully charged, the corresponding droop characteristics is like the one shown in Fig. 3(a). Therefore, the output power of PV is higher than the load. Hence the PV should operate under MPPT. As shown in Fig. 11(a), the output current of the PV is decreased to 1.5 A, which is supporting the load, and the system is in Mode V.
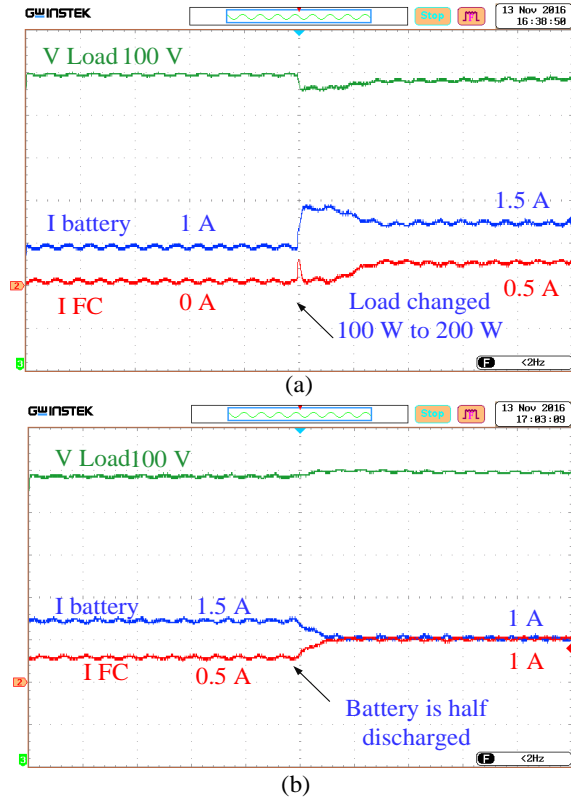

(a)

(b)

Fig. 10. Experimental results: (a) transition from Mode IV to Mode I, (b) Mode I, transition between FCC to HCC– Voltage base [10 V/div], Current base [1 A/div], Time base [50 ms/div].

In the next case, the performance of the control system is verified in the presence of battery and PV. At first, the PV is operating at MPPT with the output current of 2.05 A. The load is 150 W, and hence the PV is charging the battery with 0.6 A as shown in Fig. 11(b). The system is working in Mode IV. When the load is changed to 300 W, the battery and PV are supporting the load in Mode I.

C. Operation of battery, PV and IC:

In this test, the PV is operating at MPPT and the battery is fully charged. The dc load is 355 W. Therefore, the battery is supplying 1.5 A. The system is working in Mode I. Once the load is decreased by 110 W, the extra current of the PV is injected to the grid through the IC. And the system is operating in Mode IV. The load sharing among the PV, battery and IC is shown in Fig. 12(a). Furthermore, the output current of IC (current of inductor of filter) and the grid voltage are shown in Fig. 12(b) and Fig. 12(c).
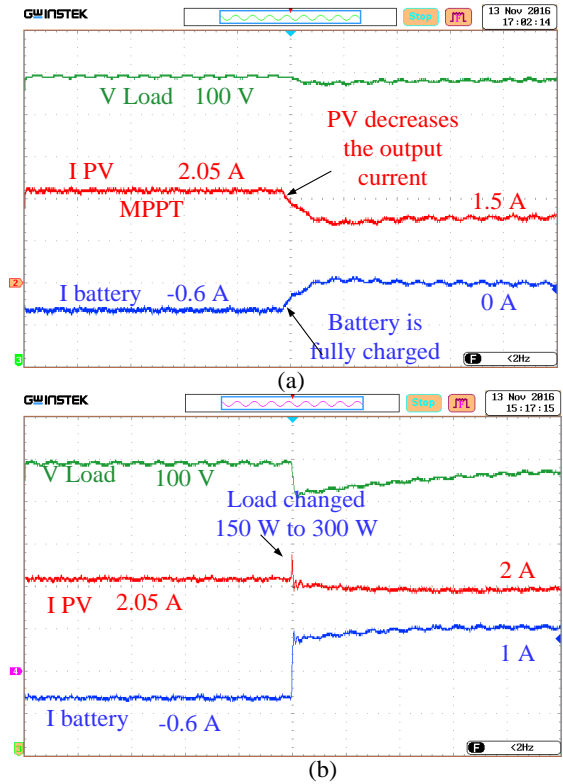

(a)

(b)

Fig. 11. Experimental results: (a) Transition from Mode IV to Mode V, (b) Transition from Mode IV to Mode I– Voltage base [10 V/div], Current base [1 A/div], Time base [50 ms/div].
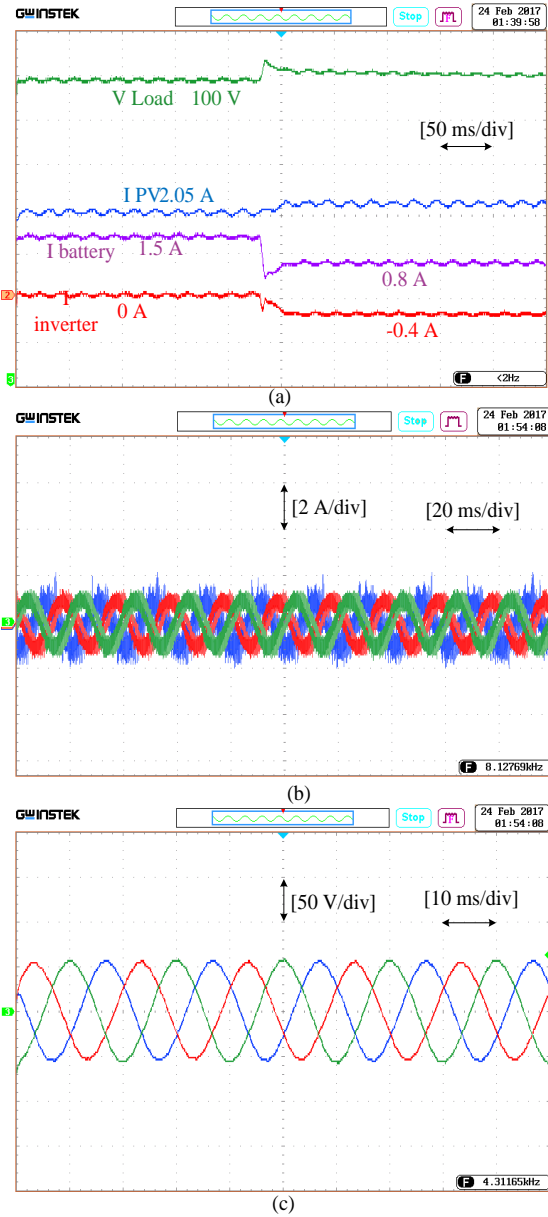
Fig. 12. Experimental Results of transition from Mode I to Mode IV: (a) dc link voltage [10 V/div], dc current of PV, battery and inverter [1 A/div], (b) ac current of inverter [2 A/div], (c) ac voltage of inverter [50 V/div].

VII. CONCLUSION

This paper has presented a novel control approach for autonomous power management in LVDC-MGs. A virtual frequency generated by the battery converters as master units is employed to proportionally control the output current of the other units as well as the exchanged power between the MG and the local grid. Unlike the dc voltage-based droop methods, the frequency-based droop approach can be employed to accurately control the output power of dispatchable and non-dispatchable units. Notably, in the absence of conventional virtual resistors, the voltage regulation is properly achieved without employing secondary controllers. Furthermore, the injected frequency has the same value all over the grid, and hence it cannot be affected by the line impedances. Moreover, the energy flow among different energy units as well as between the MG and local grid can be properly carried out

without using any extra communication network, which may introduce a better reliability. The viability of the proposed control system is ensured for different loading and sourcing conditions through the simulation. Furthermore, the proposed approach is verified by the experiment. For the future research, more than one non-dispatchable unit should be considered, and the control system needs to be generalized to manage the power of different units. Furthermore, the future power system will be made up of multi-terminal dc/ac microgrids, hence considering more than one inverter may add some new challenges to the microgrid control and operation system.

REFERENCES

[1] F. Katiraei, R. Iravani, N. Hatziargyriou, and A. Dimeas, "Microgrids Management," *IEEE Power Energy Mag.*, vol. 6, no. 3, pp. 54–65, 2008.

[2] B. T. Patterson, "DC, Come Home: DC Microgrids and the Birth of the 'Enernet,'" *IEEE Power Energy Mag.*, vol. 10, no. 6, pp. 60–69, 2012.

[3] S. Chowdhury, S. P. Chowdhury, and P. Crossley, "*Microgrids and Active Distribution Networks.*" The Institution of Engineering and Technology, 2009.

[4] B. Kroposki, R. Lasseter, T. Ise, S. Morozumi, S. Papathanassiou, and N. Hatziargyriou, "Making Microgrids Work," *IEEE Power Energy Mag.*, vol. 6, no. 3, pp. 40–53, 2008.

[5] N. Hatziargyriou, H. Asano, R. Iravani, and C. Marnay, "Microgrids," *IEEE Power Energy Mag.*, vol. 5, no. 4, pp. 78–94, 2007.

[6] S. Peyghami, H. Mokhtari, and F. Blaabjerg, "Decentralized Load Sharing in an LVDC Microgrid with an Adaptive Droop Approach Based on a Superimposed Frequency," *IEEE J. Emerg. Sel. Top. Power Electron.*, no. To be Published, DOI: 10.1109/JESTPE.2017.2674300, 2017.

[7] D. Boroyevich, I. Cvetkovic, R. Burgos, and D. Dong, "Intergrid: A Future Electronic Energy Network?," *IEEE J. Emerg. Sel. Top. Power Electron.*, vol. 1, no. 3, pp. 127–138, 2013.

[8] S. Peyghami-Akhuleh, H. Mokhtari, P. Davari, P. Chang Loh, and F. Blaabjerg, "Smart Power Management of DC Microgrids in Future Milligrids," in *Proc. IEEE EPE ECCE Europe*, 2016, pp. 1–10.

[9] D. M. Akhil, Abbas A., Georgianne Huff, Aileen B. Currier, Benjamin C. Kaun, "*DOE/EPRI 2013 Electricity Storage Handbook in Collaboration with NRECA,*" no. July. 2013.

[10] S. Peyghami, P. Davari, H. Mokhtari, P. C. Loh, and F. Blaabjerg, "Synchronverter-Enabled DC Power Sharing Approach for LVDC Microgrids," *IEEE Trans. Power Electron.*, vol. 32, no. 10, pp. 8089–8099, Oct. 2017.

[11] S. Peyghami, H. Mokhtari, P. Davari, P. C. Loh, and F. Blaabjerg, "On Secondary Control Approaches for Voltage Regulation in DC Microgrids," *IEEE Trans. Ind. Appl.*, no. 1: To be Published, DOI: 10.1109/TIA.2017.2704908, pp. 1–1, 2017.

[12] B. Luis and E. Zubieta, "Are Microgrids the Future of Energy ?," *IEEE Electrif. Mag.*, vol. 4, no. 2, pp. 37–44, 2016.

[13] Y. Gu, W. Li, and X. He, "Frequency-Coordinating Virtual Impedance for Autonomous Power Management of DC Microgrid," vol. 30, no. 4, pp. 2328–2337, 2015.

[14] Y. Gu, X. Xiang, W. Li, and X. He, "Mode-Adaptive Decentralized Control for Renewable DC Microgrid With Enhanced Reliability and Flexibility," *IEEE Trans. Power Electron.*, vol. 29, no. 9, pp. 5072–5080, 2014.

[15] T. Dragičević, J. M. J. Guerrero, J. C. Vasquez, T. Dragicevic, J. M. J. Guerrero, and J. C. Vasquez, "A Distributed Control Strategy for Coordination of an Autonomous LVDC Microgrid Based on Power-Line Signaling," *IEEE Trans. Ind. Electron.*, vol. 61, no. 7, pp. 3313–3326, Jul. 2014.

[16] X. Yu, A. Huang, R. Burgos, J. Li, and Y. Du, "A Fully Autonomous Power Management Strategy for DC Microgrid Bus Voltages," *in Proc. IEEE APEC*, pp. 2876–2881, 2013.

[17] T. Dragicevic, J. M. Guerrero, J. C. Vasquez, and D. Skrlec, "Supervisory Control of an Adaptive-Droop Regulated DC Microgrid with Battery Management Capability," *IEEE Trans. Power Electron.*, vol. 29, no. 2, pp. 695–706, 2014.

[18] T. Morstyn, S. Member, B. Hredzak, S. Member, G. D. Demetriades,

V. G. Agelidis, and S. Member, "Unified Distributed Control for DC Microgrids Operating Modes," *IEEE Trans. Power Syst.*, vol. 31, no. 1, pp. 802–812, 2016.

[19] D. Chen and L. Xu, "Autonomous DC Voltage Control of a DC Microgrid with Multiple Slack Terminals," *IEEE Trans. Power Syst.*, vol. 27, no. 4, pp. 1897–1905, Nov. 2012.

[20] J. He and Y. W. Li, "Analysis, Design, and Implementation of Virtual Impedance for Power Electronics Interfaced Distributed Generation," *IEEE Trans. Ind. Appl.*, vol. 47, no. 6, pp. 2525–2538, 2011.

[21] P.-H. Huang, P.-C. Liu, W. Xiao, and M. S. El Moursi, "A Novel Droop-Based Average Voltage Sharing Control Strategy for DC Microgrids," *IEEE Trans. Smart Grid*, vol. 6, no. 3, pp. 1096–1106, May 2015.

[22] Y. W. Li and C.-N. Kao, "An Accurate Power Control Strategy for Power-Electronics-Interfaced Distributed Generation Units Operating in a Low-Voltage Multibus Microgrid," *IEEE Trans. Power Electron.*, vol. 24, no. 12, pp. 2977–2988, Dec. 2009.

[23] X. Lu, J. M. Guerrero, K. Sun, and J. C. Vasquez, "An Improved Droop Control Method for DC Microgrids Based on Low Bandwidth Communication With DC Bus Voltage Restoration and Enhanced Current Sharing Accuracy," *IEEE Trans. Power Electron.*, vol. 29, no. 4, pp. 1800–1812, Apr. 2014.

[24] V. Nasirian, A. Davoudi, F. L. Lewis, and J. M. Guerrero, "Distributed Adaptive Droop Control for Dc Disribution Systems," *IEEE Trans. Energy Convers.*, vol. 29, no. 4, pp. 944–956, 2014.

[25] H. Nikkhajoei and R. Iravani, "Steady-State Model and Power Flow Analysis of Electronically-Coupled Distributed Resource Units," *IEEE Power Eng. Soc. Gen. Meet. PES*, vol. 22, no. 1, pp. 721–728, Jan. 2007.

[26] S. Peyghami-Akhuleh, H. Mokhtari, P. C. Loh, and F. Blaabjerg, "Distributed Secondary Control in DC Microgrids with Low-Bandwidth Communication Link," in *Proc. IEEE PEDSTC*, 2016, p. 641–645.

[27] S. Anand, B. G. Fernandes, and J. M. Guerrero, "Distributed Control to Ensure Proportional Load Sharing and Improve Voltage Regulation in Low-Voltage DC Microgrids," *IEEE Trans. Power Electron.*, vol. 28, no. 4, pp. 1900–1913, 2013.

[28] Q. Shafiee, T. Dragicevic, J. C. Vasquez, and J. M. Guerrero, "Hierarchical Control for Multiple DC-Microgrids Clusters," *IEEE Trans. Energy Convers.*, vol. 29, no. 4, pp. 922–933, 2014.

[29] X. Lu, J. M. Guerrero, K. Sun, J. C. Vasquez, R. Teodorescu, and L. Huang, "Hierarchical Control of Parallel AC-DC Converter Interfaces for Hybrid Microgrids," *IEEE Trans. Smart Grid*, vol. 5, no. 2, pp. 683–692, 2014.

[30] S. Peyghami, H. Mokhtari, P. C. Loh, P. Davari, and F. Blaabjerg, "Distributed Primary and Secondary Power Sharing in a Droop-Controlled LVDC Microgrid with Merged AC and DC Characteristics," *IEEE Trans. Smart Grid*, no. To be Published, DOI: 10.1109/TSG.2016.2609853, 2016.

[31] J. Rocabert, A. Luna, F. Blaabjerg, and P. Rodriguez, "Control of Power Converters in AC Microgrids," *IEEE Trans. Power Electron.*, vol. 27, no. 11, pp. 4734–4749, 2012.

[32] P. C. Loh, Y. K. Chia, D. Li, and F. Blaabjerg, "Autonomous Operation of Distributed Storages in Microgrids," *IET Power Electron.*, vol. 7, no. 1, pp. 23–30, 2014.

Saeed Peyghami (S'14) was born in Tabriz, Iran, in 1988. He received the B.Sc., M.Sc. and Ph.D. degrees all in electrical engineering from the Department of Electrical Engineering, Sharif University of Technology, Tehran, in 2010, 2012, and 2017 respectively.

He stayed at the Department of Energy Technology in Aalborg University as a visiting scholar from 2015 to 2016. From 2016 to 2017, he worked at Sharif Industrial Development Center as a senior electrical engineer. His research interests include power electronics system control, power quality, application of power electronics in distributed power systems.

Hossein Mokhtari (M'03–SM'14) was born in Tehran, Iran, on August 19, 1966. He received the B.Sc. degree in electrical engineering from Tehran University, Tehran, in 1989. He received the M.Sc. degree in power electronics from the University of New Brunswick, Fredericton, NB, Canada, in 1994, and the Ph.D. degree in power electronics/power quality from the University of Toronto, Toronto, ON, Canada in 1999.

From 1989 to 1992, he worked in the Consulting Division of Power Systems Dispatching Projects, Electric Power Research Center Institute, Tehran. Since 2000, he has been with the Department of Electrical Engineering, Sharif University of Technology, Tehran, where he is currently a Professor. He is also a Senior Consultant to several utilities and industries.

Frede Blaabjerg (S'86–M'88–SM'97–F'03) was with ABB-Scandia, Randers, Denmark, from 1987 to 1988. From 1988 to 1992, he was a Ph.D. Student with Aalborg University, Aalborg, Denmark. He became an Assistant Professor in 1992, Associate Professor in 1996, and Full Professor of power electronics and drives in 1998. His current research interests include power electronics and its applications such as in wind turbines, PV systems, reliability, harmonics and adjustable speed drives.

He has received 17 IEEE Prize Paper Awards, the IEEE PELS Distinguished Service Award in 2009, the EPE-PEMC Council Award in 2010, the IEEE William E. Newell Power Electronics Award 2014 and the Villum Kann Rasmussen Research Award 2014. He was an Editor-in-Chief of the IEEE TRANSACTIONS ON POWER ELECTRONICS from 2006 to 2012. He is nominated in 2014 and 2015 by Thomson Reuters to be between the most 250 cited researchers in Engineering in the world.